Impact of ALD grown passivation layers on silicon nitride based integrated optic devices for very-near-infrared wavelengths

Amit Khanna,[1,4,*] Ananth Z Subramanian,[1] Markus Häyrinen,[2] Shankar Selvaraja,[3] Peter Verheyen,[3] Dries Van Thourhout,[1] Seppo Honkanen,[2] Harri Lipsanen,[4] and Roel Baets[1]

[1]*Photonics Research Group, Ghent University-imec, Center for Nano- and Biophotonics, Ghent University, Ghent 9000, Belgium*
[2]*Institute of Photonics, University of Eastern Finland, FI-80101 Joensuu, Finland*
[3]*Imec, Kapeldreef 75, Leuven 3001, Belgium*
[4]*Department of Micro and Nanosciences, School of Electrical Engineering, Aalto University, Finland, Espoo 02150 Finland*
[*]*amit.khanna@imec.be*

Abstract: A CMOS compatible post-processing method to reduce optical losses in silicon nitride (Si_3N_4) integrated optical waveguides is demonstrated. Using thin layer atomic layer deposition (ALD) of aluminum oxide (Al_2O_3) we demonstrate that surface roughness can be reduced. A 40 nm thick Al_2O_3 layer is deposited by ALD over Si_3N_4 based strip waveguides and its influence on the surface roughness and the waveguide loss is studied. As a result, an improvement in the waveguide loss, from very high loss (60 dB/cm) to low-loss regime (~5 dB/cm) is reported for a 220 nm x 500 nm Si_3N_4 wire at 900 nm wavelength. This opens prospects to implement very low loss waveguides.

References and links

1. A. Gorin, A. Jaouad, E. Grondin, V. Aimez, and P. Charette, "Fabrication of silicon nitride waveguides for visible-light using PECVD: A study of the effect of plasma frequency on optical properties," Opt. Express **16**(18), 13509–13516 (2008).
2. J. N. Milgram, J. Wojcik, P. Mascher, and A. P. Knights, "Optically pumped Si nanocrystal emitter integrated with low loss silicon nitride waveguides," Opt. Express **15**(22), 14679–14688 (2007).
3. K. Ikeda, R. E. Saperstein, N. Alic, and Y. Fainman, "Thermal and Kerr nonlinear properties of plasma-deposited silicon nitride/ silicon dioxide waveguides," Opt. Express **16**(17), 12987–12994 (2008).
4. A. Gondarenko, J. S. Levy, and M. Lipson, "High confinement micron-scale silicon nitride high Q ring resonator," Opt. Express **17**(14), 11366–11370 (2009).
5. F. Morichetti, A. Melloni, M. Martinelli, R. G. Heideman, A. Leinse, D. H. Geuzebroek, and A. Borreman, "Box-shaped dielectric waveguides: a new concept in integrated optics," J. Lightwave Technol. **25**(9), 2579–2589 (2007).
6. N. Daldosso, M. Melchiorri, F. Riboli, M. Girardini, G. Pucker, M. Crivellari, P. Bellutti, A. Lui, and L. Pavesi, "Comparison among various Si_3N_4 waveguide geometries grown within a CMOS fabrication pilot line," J. Lightwave Technol. **22**(7), 1734–1740 (2004).
7. J. S. Levy, A. Gondarenko, M. A. Foster, A. C. Turner-Foster, A. L. Gaeta, and M. Lipson, "CMOS-compatible multiple-wavelength oscillator for on-chip optical interconnects," Nat. Photonics **4**(1), 37–40 (2010).
8. L. Razzari, D. Duchesne, M. Ferrera, R. Morandotti, S. Chu, B. E. Little, and D. J. Moss, "CMOS-compatible integrated optical hyper-parametric oscillator," Nat. Photonics **4**(1), 41–45 (2010).
9. F. Ferdous, H. Miao, D. E. Leaird, K. Srinivasan, J. Wang, L. Chen, L. T. Varghese, and A. M. Weiner, "Spectral line-by-line pulse shaping of on-chip microresonator frequency combs," Nat. Photonics **5**(12), 770–776 (2011).
10. S. Romero-García, F. Merget, F. Zhong, H. Finkelstein, and J. Witzens, "Silicon nitride CMOS-compatible platform for integrated photonics applications at visible wavelengths," Opt. Express **21**(12), 14036–14046 (2013).

11. R. Halir, Y. Okawachi, J. S. Levy, M. A. Foster, M. Lipson, and A. L. Gaeta, "Ultrabroadband supercontinuum generation in a CMOS-compatible platform," Opt. Lett. **37**(10), 1685–1687 (2012).
12. I. Goykhman, B. Desiatov, and U. Levy, "Ultrathin silicon nitride microring resonator for biophotonic applications at 970 nm wavelength," Appl. Phys. Lett. **97**(8), 081108 (2010).
13. S. Romero-García, F. Merget, F. Zhong, H. Finkelstein, and J. Witzens, "Silicon nitride CMOS-compatible platform for integrated photonics applications at visible wavelengths," Opt. Express **21**(12), 14036–14046 (2013).
14. T. Alasaarela, D. Korn, L. Alloatti, A. Säynätjoki, A. Tervonen, R. Palmer, J. Leuthold, W. Freude, and S. Honkanen, "Reduced propagation loss in silicon strip and slot waveguides coated by atomic layer deposition," Opt. Express **19**(12), 11529–11538 (2011).
15. M. Häyrinen, M. Roussey, V. Gandhi, M. Kuittinen, and S. Honkanen, "New approach to fabricate low-loss Titanium dioxide waveguides with electron beam lithography and atomic layer deposition," in Conference Paper on Advanced Photonics 2013, OSA Technical Digest (online), paper IT2A.5 (2013).
16. A. Z. Subramanian, S. Selvaraja, P. Verheyen, A. Dhakal, K. Komorowska, and R. Baets, "Near-infrared grating couplers for silicon nitride photonic wires," IEEE Photon. Technol. Lett. **24**(19), 1700–1703 (2012).
17. F. Grillot, L. Vivien, S. Laval, D. Pascal, and E. Cassan, "Size influence on the propagation loss induced by sidewall roughness in ultrasmall SOI waveguides," IEEE Photon. Technol. Lett. **16**(7), 1661–1663 (2004).
18. FIMMWAVE by Photon Design, http://www.photond.com/.
19. G. Ghosh, "Dispersion-equation coefficients for the refractive index and birefringence of calcite and quartz crystals," Opt. Commun. **163**(1-3), 95–102 (1999).

1. Introduction

Silicon nitride (Si_3N_4) exhibits bulk material transparency in the visible and infrared part of the electro-magnetic spectrum [1,2]. Si_3N_4 based devices have been demonstrated using strip and ridge waveguides, and the silicon oxynitride (SiON) based 'A-shaped' box waveguide [3–6]. Enabled by the broad spectrum transparency, moderately high refractive index (~2.0) and low-loss, Si_3N_4 based integrated optics is gaining prominence in diverse domains ranging from telecom to life sciences [7–12]. Further, Si_3N_4 leverages the advantages of the mature complementary-metal-oxide-semiconductor (CMOS) infrastructure to realize uniform and reproducible integrated optical devices within wafer and wafer-to-wafer [13]. Together, these factors have contributed to interest shown by the industry and the academia towards Si_3N_4 technology platform for photonic applications, especially in the visible and very-near-infrared (VNIR) wavelength regime (400-1000 nm). However, the path to a mature Si_3N_4 technology on the CMOS infrastructure requires foremost, the realization of passive optical devices with low-losses. In optical waveguides, scattering due to rough interfaces is the main source of loss; and especially in high-index-contrast waveguides, roughness of nm-level can lead to unacceptable waveguide losses. In this paper, a method to reduce surface roughness of the Si_3N_4 photonic wire waveguide manufactured on a 200 mm CMOS pilot-line is investigated. Non-optimized processing resulted in nanometer-scale surface roughness and consequently high propagation loss. Over such a high loss device, 40 nm alumina (Al_2O_3) is deposited by atomic layer deposition (ALD) technique. In silicon photonics the high refractive-index-contrast of silicon wire waveguides leads to strong scattering at the sidewalls and consequently high loss. Use of conformal ALD layers to reduce surface roughness and consequently reduce loss in the infrared wavelength regime (λ = 1550 nm) for silicon and titania (TiO_2) wire waveguides has been demonstrated [14,15]. Si_3N_4 strip waveguides possesses much lower material index contrast but nevertheless, at shorter wavelengths (visible-VNIR), sidewall roughness remains the major source of the waveguide loss because of the Rayleigh scattering, which is inversely proportional to the fourth power of the wavelength. Therefore, the influence of scattering on the propagation loss is expected to be more pronounced in Si_3N_4 material system at visible-VNIR wavelengths vis-à-vis silicon photonics in the infrared regime. Thus, the impact of ALD grown passivation layers on Si_3N_4 based integrated optic devices for VNIR wavelengths acquires significance. To the best of our knowledge, ALD coatings to reduce surface scattering loss in Si_3N_4 wire waveguides has not been studied earlier. In this paper, we report the influence of ALD deposition of a thin layer

of Al_2O_3 on the surface roughness and loss in a 220 nm X 500 nm Si_3N_4 based wire waveguide.

2. Waveguide processing and characterization

A 200 mm bare Si wafer is used as the substrate. Firstly, plasma enhanced chemical vapor deposition (PECVD) is used to deposit 2.4 μm silicon dioxide (SiO_2) followed by: 220 nm thick Si_3N_4 deposition using PECVD technique. The SiH_4, N_2 and NH_3 gas flows are optimized for Si_3N_4 deposition at 400 °C, which ensured CMOS back-end compatibility. After the layer deposition, the waveguide and the grating couplers (GC) are patterned by using 193 nm optical lithography and reactive-ion-etch process. The waveguide is deeply etched (220 nm deep), and the GCs are defined with different etch-depths by controlling the etch duration. Photoresist is used as an etch mask for both the etch processes. After dry etching, the wafers are cleaned by using oxygen plasma and a wet chemical process. The widths of the waveguides are in the range of 500 ± 30 nm. Since Si_3N_4 does not have any absorption band near 900 nm wavelength band, no heat treatment is applied to these wafers. At the end, the dies are diced from the wafer for optical characterization.

After dicing, an Al_2O_3 film is deposited over a batch of Si_3N_4 chips by ALD process. In this ALD process a 40 nm film of Al_2O_3 is grown at 120 °C by using Trimethyl Aluminium (TMA) and water (H_2O) as precursors with ALD TFS 200 equipment by Beneq. Simultaneously, a silicon dummy sample is coated in the same chamber and it is used for characterization of the ALD grown film.

The refractive index of 220 nm Si_3N_4 and 40 nm Al_2O_3 are determined using ellipsometry before and after ALD deposition, respectively. The roughness of the waveguide surface is compared prior-to and after 40 nm Al_2O_3 deposition using atomic force microscopy (AFM). The propagation loss in the 500 nm wide wire is compared by cut-back method using spiral waveguides of different lengths (1, 2, 4 and 7 cm). For accurately characterizing waveguide propagation loss, all the spirals are designed to have the same number of bends and bend radius. Besides, the same spirals are used before and after ALD deposition for accurately determining the effect of ALD deposition of alumina on the waveguide propagation loss. These measurements are performed for the TE polarization using a tunable laser source emitting in the range 890–910 nm and a single mode fiber at this wavelength range. Due to the limited bandwidth of the tunable laser source the grating coupler measurements are performed by coupling unpolarized light from a tungsten halogen white light source (400 nm –1700 nm) using a single mode fiber into the waveguides. Another similar fiber is positioned above the output GC to collect the light into an optical spectrum analyzer. The coupling efficiency is determined from the fiber-to-fiber transmission. The position of the fiber is optimized for maximum transmission.

3. Experimental results and discussion

Si_3N_4 waveguides

The material refractive index of the Si_3N_4 waveguides is determined by ellipsometry measurements on the Si_3N_4 as-deposited films. Figure 1 shows the refractive index vs. wavelength results as determined by ellipsometry measurements. An index of 2.018 at 900 nm is measured by the ellipsometry experiment.
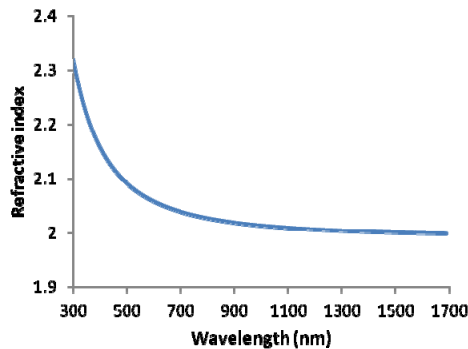
Fig. 1. Refractive index as determined by ellipsometry of Si₃N₄ thin film.

To ascertain the deposited thicknesses of the layers after fabrication, focused ion beam (FIB) milling with Ga-ions is used to produce cross-sections of the waveguides and underlying PECVD SiO$_2$. The cross-sections are analyzed using scanning electron microscope (SEM). SEM micrographs show the thickness of Si$_3$N$_4$ to be 230 ± 15 nm for a targeted value of 220 nm Si$_3$N$_4$. The nominal width (on the mask) of the waveguide is 500 nm and the measured width is in close correspondence with the targeted value. As shown in Fig. 2(a) the thickness of PECVD deposited oxide is 2.43 µm. Figure 2(b) shows the cross-section of the GC used in the experiments with a targeted etch depth of 140 nm and a period of 630 nm. In Fig. 2(c) the strip waveguide cross-section is shown. In order to avoid excessive charging effects, the chips are coated with gold before SEM measurements.
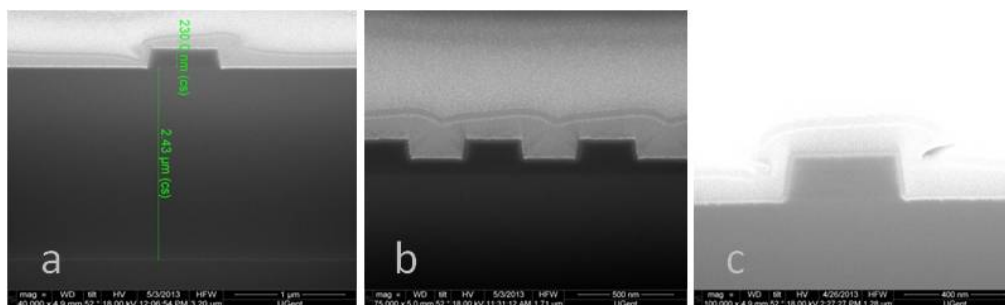

Fig. 2. SEM micrographs of the Si$_3$N$_4$ device cross-sections prepared using FIB milling. (a) 220 nm x 500 nm Si$_3$N$_4$ wire along with underlying SiO$_2$. (b) Grating coupler with 140 nm partial etch depth, 630 nm period. (c) 220 nm x 500 nm Si$_3$N$_4$ wire.

The cut-back measurement on these waveguides is performed to determine propagation loss in the waveguides. The results show extremely high total loss, greater than 60 dB with some measurements being very close to noise floor of the detector (Table 1). Therefore, these cut back measurements could not be trusted for accurate determination of waveguide loss. This high value of total loss is attributed to the coupling loss of the gratings, bend losses and very high propagation loss of the waveguide due to rough surface of the sidewall and buried oxide layer. Substrate coupling is negligible since the buried oxide thickness (2.4 μm) is sufficient to decouple a 500 nm wide wire from the underlying substrate.

To study such high total losses, Si$_3$N$_4$ waveguides are analyzed using AFM to investigate the quality of the waveguide surface in terms of surface roughness. Accurate determination of sidewall roughness is challenging, therefore the surface roughness over the 220 nm high surface of the grating couplers is measured as an indicative measure of the surface quality. In Table 1, the measured data is shown. The measured RMS roughness is 1.73 nm with a peak-to-peak roughness of about 9.19 nm.

Table 1. Loss measurement results for air clad samples obtained via cut-back measurements are shown. Roughness data of the waveguides obtained by AFM analysis of waveguide surface is also shown. For comparison, loss and surface roughness data of air clad samples fabricated by a different etch recipe and reported in [16] are presented.

Sample	Parameter	Measured Data
Air Clad Samples	Loss, dB/cm	Indeterminable
	Excess Loss (Y-intercept), dB	>60
	Root mean square roughness (Rq)	1.73 nm
	Maximum height of the roughness (Rt)	9.19 nm
Air Clad Samples [16]	Loss, dB/cm	4.0
	Root mean square roughness (Rq):	0.5 nm
	Maximum height of the roughness (Rt):	2.2 nm

For comparison, PECVD Si_3N_4 waveguides of similar dimensions but fabricated using different etching mechanism are also analyzed using AFM. These waveguides exhibit a waveguide loss of 4 dB/cm and were reported by co-authors previously [16]. The AFM results for these waveguides are also shown in Table 1. The measured RMS roughness is 0.5 nm with a peak-to-peak roughness of about 2.2 nm.

Si_3N_4 waveguides with 40 nm Al_2O_3 ALD

To reduce losses by reduction of surface roughness we deposit an Al_2O_3 thin film by the ALD technique as described in Sec 2. During ALD deposition a dummy sample is placed with the Si_3N_4 device chips to characterize the deposited Al_2O_3 thin film. The material refractive index of the Al_2O_3 layer is determined by ellipsometry to be n = 1.559 +/− 0.003 at 900 nm wavelength. The selection of Al_2O_3 as the ALD material for deposition is based on its material refractive index at λ = 900 nm which is suited for gradually lowering the refractive index between air (n = 1) and Si_3N_4 (n~2). The thickness of the deposited Al_2O_3 is 39.9 nm as shown in Fig. 3(a). Device cross-section imaging under SEM is limited by lower contrast between secondary electrons scattered by Al_2O_3 and Si_3N_4 layers in the SEM. These SEM measurements have an in-accuracy of ~+/−5 nm. The choice of thin film thickness for ALD Al_2O_3 is based on the simulation results of the conformal deposition of thin films over rough surfaces in [14]. The simulation shows reduction of the RMS surface roughness by 1 nm through 40 nm conformal thin film deposition. Since such thickness is sufficient to bring surface roughness to levels shown in Table 1 (air clad samples [16]), 40 nm growth of Al_2O_3 by ALD is used. Further, due to wavelength equivalence ($\lambda/n_{eff[TE]}$) of 900 nm wavelength within Si_3N_4 wire (n~2, $\lambda/n_{eff[TE]}$ = 580 nm) with 1550 nm wavelength within silicon wire (n~3.5, $\lambda/n_{eff[TE]}$ = 640 nm) the 40 nm ALD film is expected to be equally if not more suitable to reduce losses due to surface scattering, as shown in Table 2.

Table 2. Wavelength equivalence between Si wire and Si_3N_4 wire at 1550 nm and 900 nm wavelengths, respectively. Wire geometry 500 nm X 220 nm.

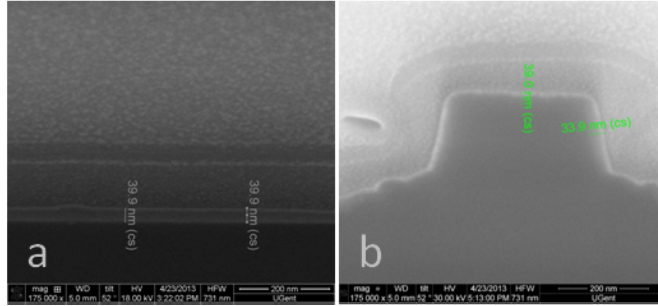| Parameter	Si	Si_3N_4
λ (nm)	1550	900
n_{eff} (quasi-TE mode)	2.42	1.56
$\lambda/n_{eff[TE]}$ (nm)	640	577

Fig. 3. SEM micrographs of the 40 nm Al_2O_3 ALD clad Si_3N_4 waveguide cross-sections prepared using FIB milling. (a): SEM cross section image of the dummy sample placed in the chamber during ALD deposition, measured thickness of deposited Al_2O_3 is 39.9 nm. (b) Lower contrast SEM image of deposited Al_2O_3 over the Si_3N_4 waveguide.

The surface roughness of the Al_2O_3 ALD-coated Si_3N_4 chips is reanalyzed using AFM scan over the grating couplers. The surface roughness is expectedly reduced as shown in Table 3. The RMS surface roughness is measured to be 0.42 nm reduced from 1.73 nm while the maximum height of roughness is 2.25 nm reduced from 9.19 nm before ALD deposition of Al_2O_3 (Table 1, air clad samples). Further, 40 nm Al_2O_3 ALD coated Si_3N_4 devices exhibit roughness parameters comparable to the previously reported Si_3N_4 waveguides with a loss of about 4 dB/cm as shown for air clad samples [16], in Table 1.

Table 3. Average RMS and average maximum peak-to-peak surface roughness data obtained by AFM for Chip1 and Chip2 after 40 nm Al_2O_3 ALD deposition. Propagation loss (dB/cm) and excess-loss (dB) obtained by cut-back measurements after ALD deposition over Chip1 and Chip2 is also shown.

Sample	Parameter	Measured Data
Avg. [Chip 1, Chip2]	Root mean square roughness (nm)	0.42
Avg. [Chip 1, Chip2]	Maximum height of the roughness (nm)	2.25
Chip 1	Loss (dB/cm)	4.90
	Excess loss (dB)	28.77
Chip 2	Loss (dB/cm)	5.78
	Excess loss (dB)	31.98

In order to study the effect of ALD on waveguide loss, two chips measured previously (Table 1, air clad samples with indeterminable loss) are ALD coated with 40 nm Al_2O_3 and re-measured using cut-back method. The result of these measurements is shown in Fig. 4. Firstly, both the dies show much reduced excess loss as shown in Table 3. Secondly, the measurements are performed well above the noise floor of the detector thereby making the cut-back measurements reliable. Chip1 exhibited a waveguide loss of 4.90 dB/cm whereas Chip2 showed a loss of 5.78 dB/cm (Table 3). Waveguide propagation loss similar to previously reported Si_3N_4 waveguides in [16] is shown in Fig. 4 for ALD Al_2O_3 coated Si_3N_4 waveguides.
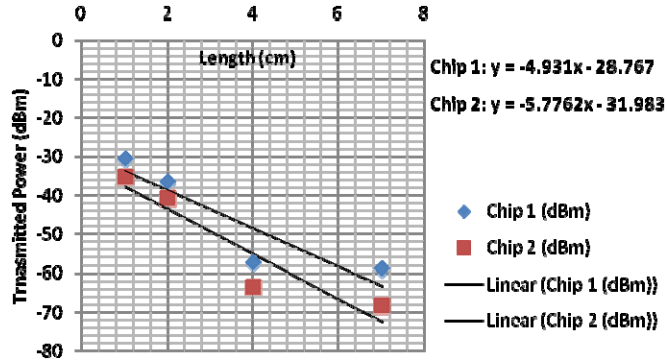
Fig. 4. Graph shows cut-back measurement results after 40 nm ALD deposition of Al_2O_3. Chip1 and Chip2 exhibit much reduced loss of 4.9 dB/cm and 5.8 dB/cm, respectively.

In order to ascertain the origin of ~30 dB excess loss in the cut-back method (Table 3) and the influence of GCs, white light measurements are used to characterize the gratings. The results show that the loss due to grating couplers at 900 nm wavelength is 20 dB, 10 dB per GC. After 40 nm ALD deposition the peak resonance of the grating is expected to shift by <5 nm which is within the 1 dB bandwidth of the gratings. For the loss measurement same wavelength and angle of incidence was used to characterize the waveguides. The remaining 10 dB loss is attributed to the bends in the spiraling waveguides which have a bend radius of 10 um. For Si_3N_4 waveguides the minimum bend radius for almost lossless transmission is estimated to be 25 μm. The third spiral (4 cm long) is observed to have some debris on top of the waveguide acquired either during cleaving or the fabrication itself. It was not possible to clean it and as a result, it led to excess scattering and deviation for both the chips from the straight-line fit of the collected transmitted power. The location and optical impact of the debris was indeterminable prior to ALD deposition due to total losses being close to noise floor at that stage.

4. Discussion

Optical images of the Si_3N_4 chips prior-to and after ALD coating of 40 nm Al_2O_3 film are obtained using a CMOS camera. Images shown in Fig. 5 are obtained at the same magnification of the microscope and similar ambient brightness, thus reducing the variations due to the camera set-up and environment. Care was taken not to saturate the camera by working at lower power. A comparison of these images clearly indicates the reduction in the light scattering from the waveguides after ALD deposition. By measuring the decay in the light intensity along the length of the waveguide propagation loss due to scattering before and after ALD coating is estimated, as shown in Fig. 5. Hot-spots leading to sudden peaks in this measurement were unavoidable but the waveguide propagation loss estimate from the measurement corresponded well with the loss estimated using cutback method. The experiment indicates extremely high waveguide propagation loss prior-to ALD coating (~60 dB/cm) whereas the loss after ALD coating is ~6 dB/cm, which re-confirms the loss measured by the cut back method (Table 3).
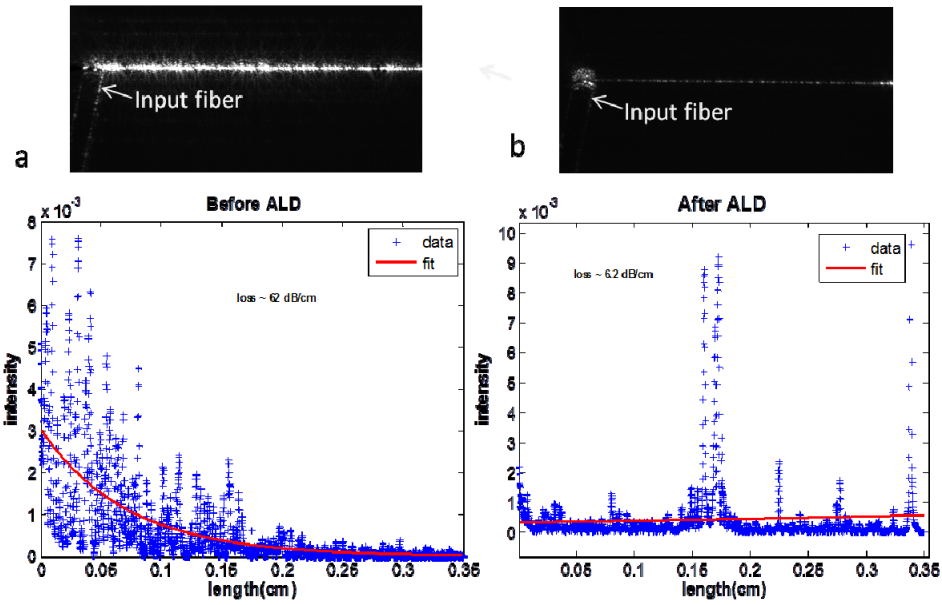
Fig. 5. (Top) Image captured through an optical microscope of Si_3N_4 wire conducting light coupled through a grating coupler. (Below) Corresponding intensity decay plot to determine loss. (a) Air clad waveguide, 62 dB/cm and (b) 40 nm Al_2O_3 ALD coated Si_3N_4 waveguide, 6.2 dB/cm.

The relation between surface roughness and waveguide losses is dependent on the waveguide width [17]. In the single mode regime, as the waveguide geometry approaches the mode cut-off the scattering loss increases exponentially due to the decrease in the optical mode confinement within the waveguide and the increase in the interaction of the electrical fields of the optical mode with the rough waveguide surface. Larger waveguide cross-section geometries are above cut-off, therefore impact of scattering loss is reduced due to the high mode confinement within the waveguide. Further, it is also believed that the ALD deposition will reduce the surface roughness of the silica substrate proximal to the waveguide which may be rough due to timed dry etch recipe used for 220 nm deep nitride etch. This may also contribute towards reducing waveguide propagation losses. To study the impact of ALD deposited 40 nm Al_2O_3 on the optical mode distribution and optical field confinement, Fimmwave [18], a commercially available mode solver is used. For the simulations, a Si_3N_4 waveguide cross-section of 220 nm X 500 nm covered by 40 nm Al_2O_3 is studied. Silica (SiO_2) is used as substrate. The simulation window size is 2 μm X 2 μm while film mode matching method (FMM) is used for the simulations. Material indices used for simulations are determined using ellipsometry as described in Section 2. For SiO_2 material refractive index of 1.54 is used from literature [19].

The simulation results show smaller amplitude of the dominant E_x-component of the electrical field for quasi-TE mode at the Si_3N_4-Al_2O_3 interface as shown in Fig. 6(b) compared with the Si_3N_4-air interface as shown in Fig. 6(a). This is due to the smaller refractive-index-contrast at the Si_3N_4-Al_2O_3 vis-à-vis Si_3N_4-air material discontinuity. Furthermore, the peak amplitude of E_x in Fig. 6(b) is at Al_2O_3-air interface where surface roughness is expected to be much reduced due to the conformal ALD deposition.
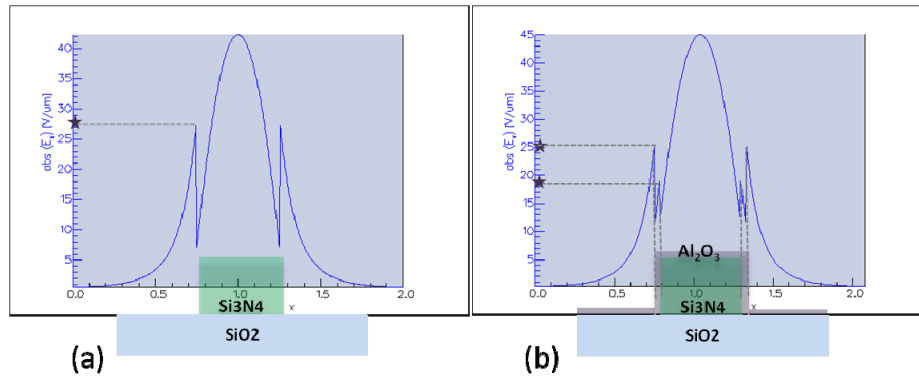
Fig. 6. E_x field distribution of the quasi-TE mode at the center of the Si_3N_4 strip waveguide are shown. On the Y-axis the E_x field amplitude are marked at critical material interfaces (a) Air clad Si_3N_4 wire showing a high E_x field amplitude at the rough, Si_3N_4-air material interface. (b) Al_2O_3 clad Si_3N_4 wire showing a lower E_x field amplitude at the rough, Si_3N_4-air material interface and a higher E_x field amplitude at the less rough Al_2O_3-air interface.

With ALD deposition, the optical mode fill-factor within the Si_3N_4 wire increases to 0.58 from 0.49 with air cladding (simulation results in Table 4). The increased optical mode confinement reduces the impact of surface roughness on the optical mode loss in the case of ALD clad waveguide.

Table 4. Comparison of fill factors in air clad and ALD coated Si_3N_4 chips.

ALD Clad Si_3N_4 Chip	Air Clad Si_3N_4 Chip
$n_{eff\,[TE]}$ = 1.6054	$n_{eff\,[TE]}$ = 1.5654
Fill Factor$_{Si3N4}$ = 0.5805	Fill Factor$_{Si3N4}$ = 0.4933

While this paper shows results on reduction from extremely high to moderately low propagation loss waveguides, the technique can also be used to reduce scattering losses from moderately low to very low propagation loss Si_3N_4 waveguides.

5. Conclusion

We demonstrate the impact of ALD-assisted conformal Al_2O_3 coating as a simple post-processing method in reducing the scattering loss in the PECVD Si_3N_4 wires (220 nm x 500 nm) at VNIR wavelengths. The RMS roughness of the nitride waveguides is reduced from 1.47 nm to 0.5 nm through this ALD coating. As a result, the waveguide loss is reduced from very high values, estimated to be ~60 dB/cm, to a moderate 5 dB/cm level at 900 nm wavelength. Both the RMS roughness and waveguide loss achieved after ALD coating is comparable to the values reported before on similar PECVD nitride waveguides at the same wavelength.

Acknowledgments